# Study of the photon flux from the night sky at La Palma and Namibia, in the wavelength region relevant for imaging atmospheric Cherenkov telescopes

S. Preuß, G. Hermann, W. Hofmann, A. Kohnle

*Max-Planck-Institut für Kernphysik, D 69029 Heidelberg, P.O. Box 103980*

**Abstract**

The level of the night sky background light at La Palma and Namibia was determined, with emphasis on the wavelength region and solid angle coverage relevant for the operation of imaging atmospheric Cherenkov telescopes. The dependence of the night sky background light both on celestial coordinates $(alt, az)$ and on galactic coordinates $(b, l)$ was measured, with an angular resolution of about $1°$. Average light levels near the zenith are similar in both locations – $2.2 \cdot 10^{12}$ to $2.6 \cdot 10^{12}$ photons per sr s m$^2$ for 300 nm $< \lambda <$ 650 nm. With increasing zenith angle the level of background light increases at La Palma, whereas a constant level is measured in Namibia. Near the center of the Milky Way, background light levels are increased by a factor up to 4 and more. Also the level of light backscattered from the ground has been studied.

*Key words:* Cherenkov telescopes, Night sky background light
*PACS:* 29.40.K, 95.55.Ka, 95.75.De

## 1 Introduction

Imaging atmospheric Cherenkov telescopes (IACTs) have emerged as the most powerful instrument for gamma-ray astronomy in the TeV energy regime. IACTs image the Cherenkov light emitted by an air shower onto a photomultiplier (PMT) camera. The orientation of the image in the camera is related to the direction of the air shower, the intensity to the energy of the primary, and the shape of image can be employed to separate electromagnetic showers induced by high-energy gamma-rays from those generated by cosmic-ray nuclei interacting in the atmosphere.

The typical yield of Cherenkov photons is roughly 100 photons $m^{-2}TeV^{-1}$, which arrive with a time dispersion of a few ns. Given this modest light yield, the light of the night-sky background, with intensities of order $10^{12}$ photons $m^{-2}s^{-1}sr^{-1}$, represents a significant limitation for the performance of IACTs. It defines the minimum Cherenkov light yield which can be reliably detected with the instrument, and hence its energy threshold. Noise in the Cherenkov image due to background light from the night sky results in additional uncertainties in the determination of image orientation, image intensity, and image shape. Finally, the background light generates a continuous DC current in the photon detectors, which may limit their lifetime and which in the case of photomultipliers may require the operation at modest gain, in order to limit the total charge accumulated on the last dynodes and the anode during the lifetime of the experiment. Variations of the night sky background light across the sky may also cause changes in the detection efficiencies, in particular once tight cuts are applied to select gamma-ray candidates, and may result in a systematic bias in ON-OFF measurements, where the rate from a background region of the sky is used to estimate the rate of background events in the signal region; care has to be taken to select signal and background regions with an identical sky brightness.

A number of different components contribute to the night sky background light and its variation with celestial and terrestrial coordinates, here given roughly in the order of their importance:

- Night airglow, which results from photochemical processes of ions in the upper atmosphere; its intensity increases with increasing zenith angle.
- The zodiacal light, which arises from the scattering of sun light by interplanetary dust near the ecliptic, and is most prominent shortly after sunset in the west, or before sunrise in the east.
- Starlight, which is partially resolved into discrete stars. The density of stars and star light varies by a large factor between the Milky Way and other regions of the sky.
- Diffuse galactic light, resulting from the scattering of star light by interstellar dust, in particular in the galactic plane.
- Extragalactic light, from unresolved galaxies and light scattered in intergalactic space represents only a very small contribution.
- Aurora, which is, however, negligible at low latitudes.

A detailed discussion of these various light sources is given in [1]; a more recent exhaustive compilation of data as well as further references can be found in [2]. Specific results for La Palma – one of the sites investigated – are given in [3].

In addition to these natural light sources, artificial light scattered in the atmosphere contributes both a continuum as well as discrete lines (Na, Hg), see

[4] for details.

Currently, a new stereoscopic IACT system - the High Energy Stereoscopic System, or H.E.S.S. ([5–7]) - is under construction in the Khomas Highland of Namibia. H.E.S.S. consists initially of four telescopes, with mirror areas of roughly 100 m$^2$ each, 15 m focal length, and cameras consisting of 960 photomultiplier tubes covering a field of view of 5° diameter. The four telescopes provide multiple views of the same shower from different perspectives, significantly enhancing the ability to reconstruct the orientation of the shower axis in space, to determine the shower energy and to reject cosmic-ray background showers. To assist in the layout of the camera and its trigger system and in the planning of observations, knowledge of the level of night-sky background is desirable.

While the night-sky background light has been extensively investigated and documented (see, e.g., [2]), it is not straight-forward to use these results to estimate the background seen by the photomultipliers of a Cherenkov telescope; one reason is that typical measurements refer to the dark sky, with no detectable stars in CCD images of large astronomical telescopes. Cherenkov telescopes with their relatively large image pixels will almost always integrate over a number of faint stars. Also, while the visibility conditions in the Gamsberg region of Namibia – near the H.E.S.S. site – have been explored extensively in earlier campaigns [8,9], little information is available about the night-sky background, and in particular about the local light pollution.

Therefore, an instrument was developed to reliably measure the yield of night sky photons in the wavelength range relevant for Cherenkov telescopes, and measurement campaigns were conducted at La Palma – the location of the HEGRA telescopes [10,11] – and in the Khomas Highland of Namibia. Results are reported in this paper. The following sections introduce the instrument and its calibration, discuss the results obtained in the two campaigns, and conclude with the implications for the H.E.S.S. telescopes.

A caveat to be mentioned is that the various components of the night-sky background light depend in differing ways on celestial and terrestrial coordinates and on time – starlight and diffuse galactic light is a function of galactic coordinates; airglow is primarily a function of terrestrial coordinates, and shows short-term as well as seasonal and solar-cycle related time variations; the zodiacal light depends on ecliptic coordinates; the contribution from artificial light sources varies with terrestrial coordinates and atmospheric conditions. Light is attenuated and scattered along its path through the atmosphere, influenced by local and large-scale atmospheric conditions. With only ground-based measurements at a given location and during a short time interval, one cannot always identify these individual contributions; it is non-trivial to interpret the results, and to judge to which extent they can be generalized. We

3

believe, however, that data were taken under rather typical conditions, and would not expect the main conclusions to change as a result of a more detailed and longer-term study.

## 2 The instrument and its calibration

In the design of an instrument to monitor the brightness of the night sky, two key choices concern the wavelength region covered, and the solid angle over which the instrument averages the photon flux.

The wavelength regime relevant for the detection of Cherenkov light is defined by the $1/\lambda^2$ distribution of the Cherenkov photons, combined with the atmospheric transmission and the quantum efficiency of the photodetectors. At short wavelengths, atmospheric transmission introduces a cutoff at about 300 nm. At long wavelengths, beyond about 500 nm, the quantum efficiency of conventional photocathodes deteriorates rapidly, and the contributions from longer wavelengths to the photoelectron yield are small. In order to directly match the sensitivity of the photon detectors of the H.E.S.S. Cherenkov cameras [12], a photomultiplier with a bi-alkali photocathode was used for the night-sky measurements. In order to test and verify the wavelength dependence of the light yield, optional narrow-band filters of 360 nm, 400 nm, 450 nm and 500 nm could be introduced in the light path.

Concerning the solid angle coverage, the relevant scales are set by the field of view of the Cherenkov cameras, with around 4° to 5° diameter, and by the field of view of the individual image elements - photomultiplier "pixels" with characteristic diameters in the range of 0.1° to 0.4°; the H.E.S.S. telescopes will use a 0.16° pixel size. The relevant level of the night-sky background is given by the average photoelectron rate induced in these pixels from dark regions of the sky; bright stars, which light up individual pixels can be handled separately. In case of the H.E.S.S. telescopes, stars between mag. 2 and 5, depending on the spectrum, will cause doubling of the typical PMT DC current, and will be clearly visible in the camera [1]. For practical reasons, it was decided to enlarge the acceptance of the instrument somewhat compared to individual pixels, and a field of view of about 0.8° effective diameter was chosen.

Fig. 1 and Fig. 2 illustrate the design of the instrument. Basically, it consists

---

[1] We note that since most Cherenkov cameras use AC-coupled readout electronics for the Cherenkov signals, the shift in the DC current due to a star imaged onto a pixel will not bias the measurement of the Cherenkov signal, as long as the PMT remains in the region of linear response; the starlight will, however, contribute increased fluctuations, i.e., noise.

of a baffled tube which defines the solid angle viewed by a photomultiplier. A remote-controlled filter wheel in front of the PMT allows to swap in the four narrow-band filters, and to cover the PMT to determine the rate of dark counts. The whole setup is mounted on a computer-controlled amateur telescope, to control the pointing (a VIXEN [2] Newtonian with 800 mm focal length and f/d = 4 on a GP-DX mount interfaced via a Skysensor 2000 PC to a portable computer running Linux). The setup furthermore includes an IR radiometer, for the purpose to detect clouds resulting in a increased IR sky temperature [13].

As PMT, the Hamamatsu HC 135 module is used, which includes a PMT with a 21 mm bi-alkali photocathode, the high voltage supply, an amplifier, discriminator, counter, timer and a control microprocessor. The unit is interfaced via a RS232 port to the portable computer. The discriminator threshold and HV are factory-preset to count signals above the "valley" of the single-photon response. The built-in processor automatically corrects dead-time during high-rate measurements.

The unit was tested and calibrated in the laboratory. The setting of the threshold was verified. Illuminating the device through a calibrated optical attenuator, the linear relation between photon flux and corrected count rate was verified at the 1% level, for count rates up to 25 MHz; in the field, measurements rates varied between 50 Hz and 5000 Hz, depending on the region of the sky viewed and the filter settings. The photon counting efficiency of the unit was determined using monochromatic light, with calibrated Hamamatsu and Newport silicon photo diodes serving as a reference, see Fig. 3. In these measurements, the photocathode was illuminated over a 10 mm diameter, similar to the diameter of the final baffle in the collimating tube. The resulting counting efficiencies are in good agreement with the calibration data at 450, 550 and 650 nm, provided with the Hamamatsu HC 135. The laboratory measurements showed a temperature dependence of the detected rate between 0.1% and 0.4% per degree Centigrade, consistent with specifications. In order to eliminate influence of temperature in the field measurements, the PMT unit was surrounded by thermal insulation, and thermostat-controlled heating resistors were used to stabilize the temperature at $22 \pm 3$ °$C$. The PMT temperature was monitored during all measurements.

The baffled tube defining the solid angle viewed by the PMT has an entrance baffle of 6.40 mm diameter, an exit baffle of 12.00 mm, and a number of intermediate baffles to reduce the influence of stray light. Fig. 4 shows the calculated transmission $\epsilon(\vartheta)$ as a function of the angle $\vartheta$ to the axis. For the calculation a point light source in the infinite is assumed and $\epsilon(\vartheta)$ is normalized

---

[2] VIXEN Optical Industries LTD., 247 Hongo, Tokorozawa, Saitama 359-0022, Japan, www.vixen.co.jp
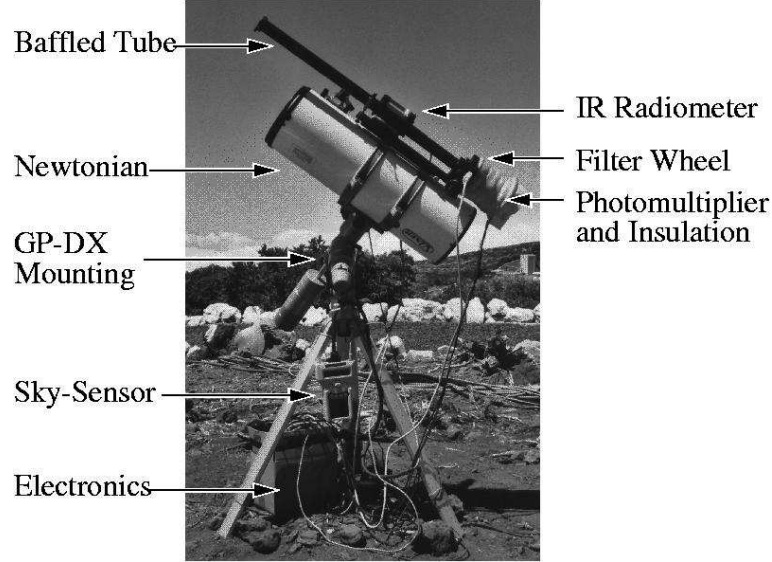
Fig. 1. Setup to measure the night sky background light, mounted on a computer-controlled amateur telescope for pointing control.
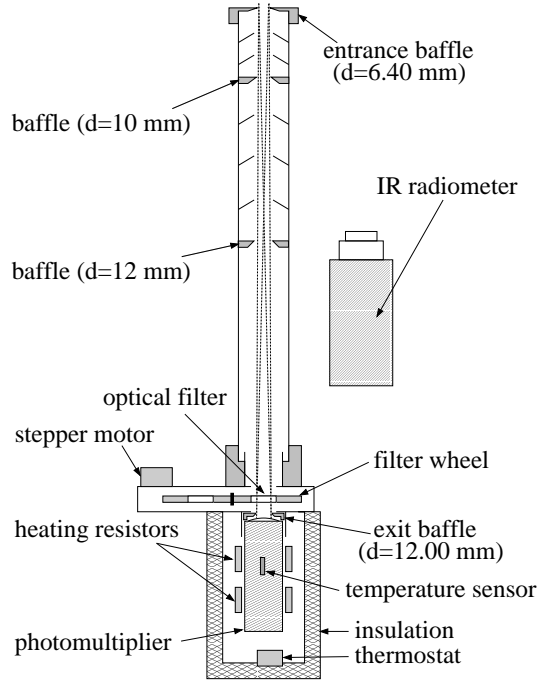


Fig. 2. The instrument consisting of a baffled tube defining the solid angle, a remote-controlled filter wheel and a temperature-controlled PMT module including a discriminator and counter.

to the amount of light incident through the entrance aperture. Integrating the transmission curve over the solid angle,

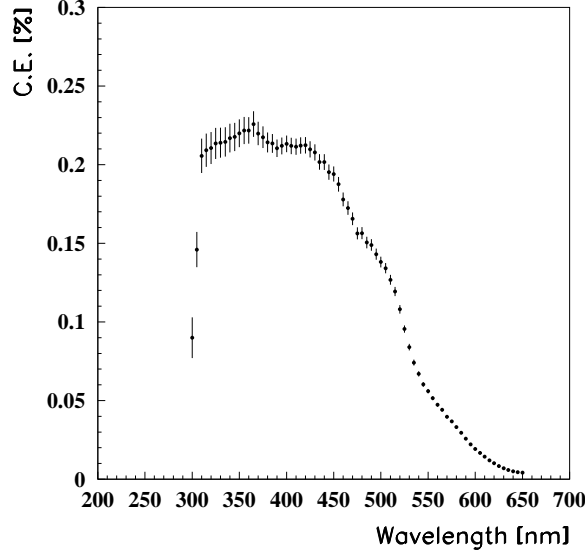$$\Omega = 2\pi \int \epsilon(\vartheta) \sin(\vartheta) \mathrm{d}\vartheta$$

Fig. 3. Measured photon counting efficiency of the PMT as a function of wavelength, using a calibrated silicon photo diode as a reference. Error bars include systematic errors.

one finds an effective solid angle coverage $\Omega$ of $(1.70\pm0.02)\cdot10^{-4}$ sr, using the geometrical dimensions given above and their errors. The effective solid angle was measured by first illuminating the bare PMT using an Ulbricht sphere with apertures of defined size in front of the PMT and the Ulbricht sphere to provide a light source of well-defined solid angle; the counting rate was determined as a function of solid angle. By measuring the rate after adding the baffle system with the Ulbricht sphere positioned to illuminate the entire field of view, the effective solid angle was then determined. From these measurements, an effective solid angle of $\Omega_{eff} = (1.79 \pm 0.05) \cdot 10^{-4}$ sr was derived, in reasonable agreement with the geometrical estimate given above. In the following, the measured value is used; it is equivalent to an effective diameter of the field of view of $0.87°$. The influence of stray light was studied by illuminating the baffled tube from different angles, and by pointing the device at a large illuminated area, where only the central spot – corresponding to the nominal aperture of the baffled tube – was blackened. After a number of iterations concerning the placement of baffles, the transmission of stray light at angles of a few degrees from the optical axis was reduced to about $10^{-5}$ of the on-axis response, corresponding to a contribution of around 1% of the signal after integration over solid angle, which should be completely uncritical. The baffled tube was aligned parallel to the telescope axis to better than $0.5°$.

The six-slot filter wheel (4 color filters, one open slot, one closed slot) is mounted at the end of the baffled tube, just before the final baffle in front of the PMT. The transmission as a function of wavelength was measured; the center wavelengths of the filters were determined to 360, 399, 448, and
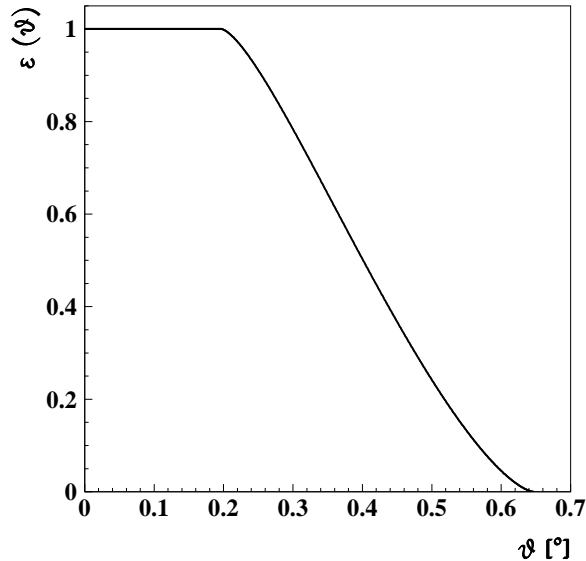
Fig. 4. Calculated transmission of the baffled tube as a function of the angle relative to the axis, normalized to the amount of light incident through the entrance aperture.

498 nm. The transmission is well described by Gaussians of width 4.3, 4.1, 3.5, and 4.3 nm, respectively. To relate count rate and photon flux, the measured transmission curves were used.

In order to test the long-term stability of the instrument and its calibration, a stable laboratory light source was employed. Measurements proved reproducible within 0.5%, even after the instrument was completely disassembled and reassembled several times.

To monitor and detect cloud layers during the measurements, an IR radiometer (Heitronics KT15.82D) was integrated into the setup. The instrument senses IR radiation in the 8 $\mu$m to 14 $\mu$m window and converts the yield into an effective sky temperature, within the limits of $-60°$C to $500°$C. The field of view of about 2° is defined by the size of the sensor combined with a germanium lens. The use of IR radiometers in sky monitoring for Cherenkov telescopes has been introduced and discussed by the Durham group [13].

In addition, the ambient temperature and the humidity were monitored during all measurements.

## 3  Determination of photon flux

A measurement results in a photon counting rate, usually averaged over 10 s. At count rates between 50 Hz and 5000 Hz, depending on the filter settings,

statistical errors are small. Dark counts – typically at a level of 20 Hz – are subtracted, but usually represent only a minor correction.

For the measurements with a narrow-band filter with center wavelength $\lambda$, the measured rate $R$ can be directly converted into a photon flux

$$\phi(\lambda) = \frac{\mathrm{d}N}{\mathrm{d}A\mathrm{d}\Omega\mathrm{d}t\mathrm{d}\lambda} = \frac{R}{A_{in}\Omega_{eff}\int T(\lambda')\epsilon_{PMT}(\lambda')\mathrm{d}\lambda'}$$

using the measured counting efficiency $\epsilon_{PMT}(\lambda)$, the filter transmission $T(\lambda)$, and the entrance area $A_{in}$ and effective solid angle $\Omega_{eff}$ of the baffled tube, under the assumption that the spectral distribution is approximately constant over the width of the filter response. Including the uncertainties in the measurements of quantum efficiencies and filter transmissions, the typical systematic errors of $\phi(\lambda)$ vary between 6.4% at 360 nm and 4.5% at 500 nm.

The measurements without filter can be presented in two ways:

- In terms of the photoelectron rate $\phi_{pe}$ per solid angle and area for bi-alkali photo cathodes,
$$\phi_{pe} = \frac{\mathrm{d}N_{pe}}{\mathrm{d}A\mathrm{d}\Omega\mathrm{d}t} = \frac{R}{A_{in}\Omega_{eff}} \quad .$$
This rate can be directly used to calculate the rate of night-sky photoelectrons in the PMTs of Cherenkov telescopes, after small corrections to account for possible differences in the peak quantum efficiency, the collection efficiency and the fraction of photoelectrons cut below the trigger threshold of the HC 135 unit.
- In terms of the integral photon rate over a certain wavelength interval, typically 300 nm to 650 nm,

$$\phi = \frac{\mathrm{d}N}{\mathrm{d}A\mathrm{d}\Omega\mathrm{d}t} = \frac{R}{A_{in}\Omega_{eff} < \epsilon_{PMT} >} \quad .$$

Here, $< \epsilon_{PMT} >$ is the counting efficiency of the PMT, averaged over the shape of the spectrum $S(\lambda)$

$$< \epsilon_{PMT} >= \int_{\lambda_1}^{\lambda_2} S(\lambda)\epsilon_{PMT}(\lambda)\mathrm{d}\lambda$$

where

$$\int_{\lambda_1}^{\lambda_2} S(\lambda)\mathrm{d}\lambda = 1 \quad .$$

The limits $\lambda_1$ and $\lambda_2$ have to be chosen such that $S(\lambda)\epsilon_{PMT}(\lambda)$ is negligible outside this range.
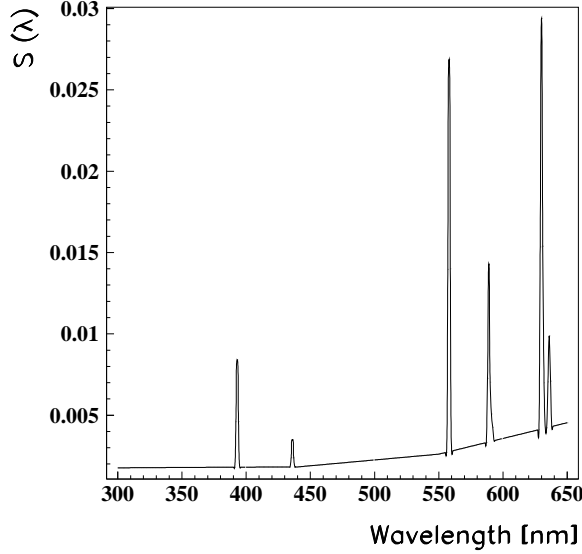
Fig. 5. Spectrum assumed in the calculation of the spectrum-averaged quantum efficiency of the PMT, following [3].

In the second case, the result obviously depends on the spectrum $S(\lambda)$ assumed for the night sky background when calculating $< \epsilon_{PMT} >$. To determine $< \epsilon_{PMT} >$, the spectrum given in [3] was used. Apart from a number of discrete lines, this spectrum is approximately flat between 300 nm to 450 nm, and rises towards longer wavelengths, see Fig. 5. The resulting average quantum efficiency is 9.8%. Including a 10% uncertainty in the shape of the assumed (normalized) spectrum, we find a systematic error of 8.8% for the integral flux. The rather extreme assumption of a constant spectrum $S(\lambda) = const$ would result in a 30% difference in the derived integral photon flux.

Alternative units used in the astronomical community to describe the level of the night sky background light are S10, the equivalent number of 10th magnitude stars per square degree, or the unit (magnitudes/arcsec$^2$). The following relations apply for the conversion [2]:

$$\phi[1/\text{sr s m}^2 \text{ nm}] = 4.80 \cdot 10^7 \phi[\text{S10 units}]$$

in the B band (440 nm), and

$$\phi[1/\text{sr s m}^2 \text{ nm}] = 3.26 \cdot 10^7 \phi[\text{S10 units}]$$

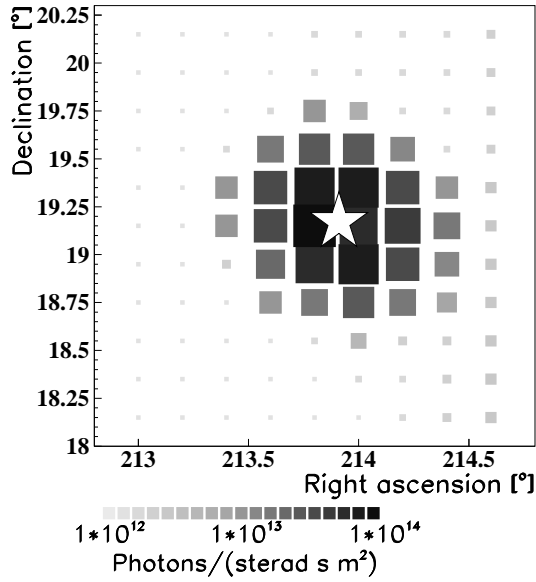in the V band (550 nm). One S10 unit in turn corresponds to 27.28 mag/arcsec$^2$.

Fig. 6. Measured photon flux in the proximity of the star Arcturus. The star in the figure denotes the nominal position of Arcturus.

## 4 Measurements of the night-sky photon flux at La Palma and Namibia

The field measurements were carried out in two campaigns at La Palma and in the Khomas Highland of Namibia. The La Palma site of the HEGRA Observatory, on the site of the Observatorio del Roque de los Muchachos, is located 2200 m asl at $17°53'24''$ W, $28°45'34''$ N. The measurements were carried out between May 18 and May 30, 2000 under good weather conditions, at temperatures between $5°$ and $15°$, and humidities between 20% and 40%. The measurements in Namibia were carried out between June 23, 2000 and July 3, 2000 on the site of the farm Hakos, about 14 km from the future site of the H.E.S.S. installation, at 1800 m asl, $16°21'28''$ E, $23°14'08''$ S. The sky was clear, and temperatures and humidity were in the same range as for the La Palma measurements.

Before each sequence of measurements, the telescope was aligned, and the alignment calibrated using three reference stars. Typical pointing precision is in the range of a few arcmin. The pointing was checked moving the instrument across a bright star, see Fig. 6. The results confirmed both the pointing and the angular response of the instrument.

Unless otherwise mentioned, all integral measurements quoted in the following refer to the wavelength range 300 nm to 650 nm. The photoelectron count rate is obtained by multiplying the flux by 0.098.

11

| Location | Ref. | Field of view (degr.) | Wavelength range (nm) | Flux $10^{12}$ $(sr\ s\ m^2)^{-1}$ | Scaled flux $10^{12}$ $(sr\ s\ m^2)^{-1}$ |
|---|---|---|---|---|---|
| La Palma | [14] | 0.43 | 300 - 600 | $1.75 \pm 0.4$ | 2.38 |
| Jammora | [15] | $\approx 0.4$ | 310 - 560 | $1.89 \pm 0.5$ | 3.33 |
| This exp., Fig. 7 | | 0.87 | 300 - 650 | | 2.2 - 2.5 |

Table 1

Other measurements of the night-sky brightness under conditions relevant for Cherenkov applications. The last column gives the photon flux scaled to the 300 - 650 nm wavelength range used in this measurement.

To determine the stability of the measured night sky brightness, a set of dark regions of the sky near the zenith was measured in several nights, and the results were averaged for each night. Fig. 7 shows the photon flux determined for 8 nights of the La Palma measurements, and for 8 nights of the Namibia campaign. The results show a scatter of about $\pm 10\%$ between nights. Since the night-to-night variation is larger than the scatter of the different measurements of a given night, this points to a systematic variation of the sky brightness. Measurements of the identical location of the sky over several hours of the same night showed a 3% rms variation of the night-sky rate. The average flux in Namibia is slightly below the average La Palma flux. Fig. 8 compares the flux at the two locations as a function of wavelength. The data can be characterized by a $\lambda^{3.5}$ dependence.

For comparison, two previous measurements of [14] and [15] specifically conducted in the framework of Cherenkov applications are summarized in Table 1; the La Palma measurement of [14] is in very good agreement with the values shown in Fig. 7; the Jammora value of [15] is higher, but consistent within errors.

The long-term median night sky brightness near the zenith at La Palma, determined from CCD images taken with the Isaac Newton and Jacobus Kapteyn telescopes, is given in [3] as 22.7 mag/arcsec$^2$ in the B band, and 21.9 mag/arcsec$^2$ in V. These values translate into $5.2 \cdot 10^9$ and $7.3 \cdot 10^9$ photons per sr s m$^2$ nm, respectively, in excellent agreement with our data (Fig. 8).

The level of the night-sky background light is a function both of the terrestrial coordinates azimuth and altitude, and of the celestial coordinates $b$ and $l$, the galactic latitude and longitude. Fig. 9 illustrates, for the Namibia location, the variation in the light yield with azimuth and altitude. In particular at low altitude, one finds a distinct variation with azimuth. The structures correspond to stray light from the city of Windhoek, at a distance of slightly over 100 km, and to a contribution from zodiacal light. In addition, data points within the galactic plane (open symbols) show an enhanced flux. The flux varies by a factor 1.5 outside the galactic plane, and is increased significantly within the
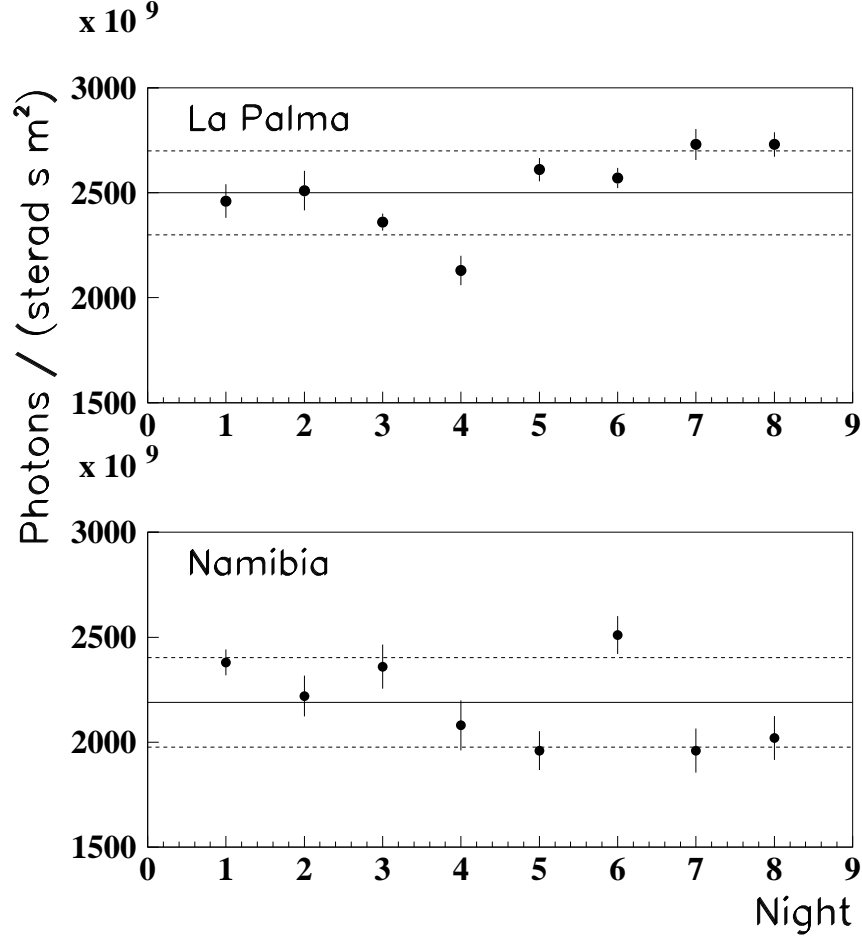
Fig. 7. Measurement of the integral photon flux from a set of dark regions near the zenith, averaged over several measurements for each single clear night, for La Palma and Namibia. The full line indicates the mean flux, the dashed lines a band of $\pm 200 \cdot 10^9$ photons/sr s m$^2$.

plane.

Of special interest was the variation of night sky brightness with altitude; the visual impression was that the sky in Namibia was very dark and clear down to the lowest altitudes. To separate in one specific case the dependence on terrestrial and celestial coordinates, two dark regions of the sky with fixed $b, l$ were measured both from Namibia and from La Palma, and were followed over a large range in altitude. The results are summarized in Fig. 10. Whereas at La Palma the night sky flux increases with decreasing altitude, the Namibia data show a constant flux down to relatively low altitude [3].

---

[3] The altitude-dependence in the La Palma data for the two selected regions is somewhat steeper than observed on average in $alt - az$ scans at La Palma; the scans, however, show qualitatively the same feature.
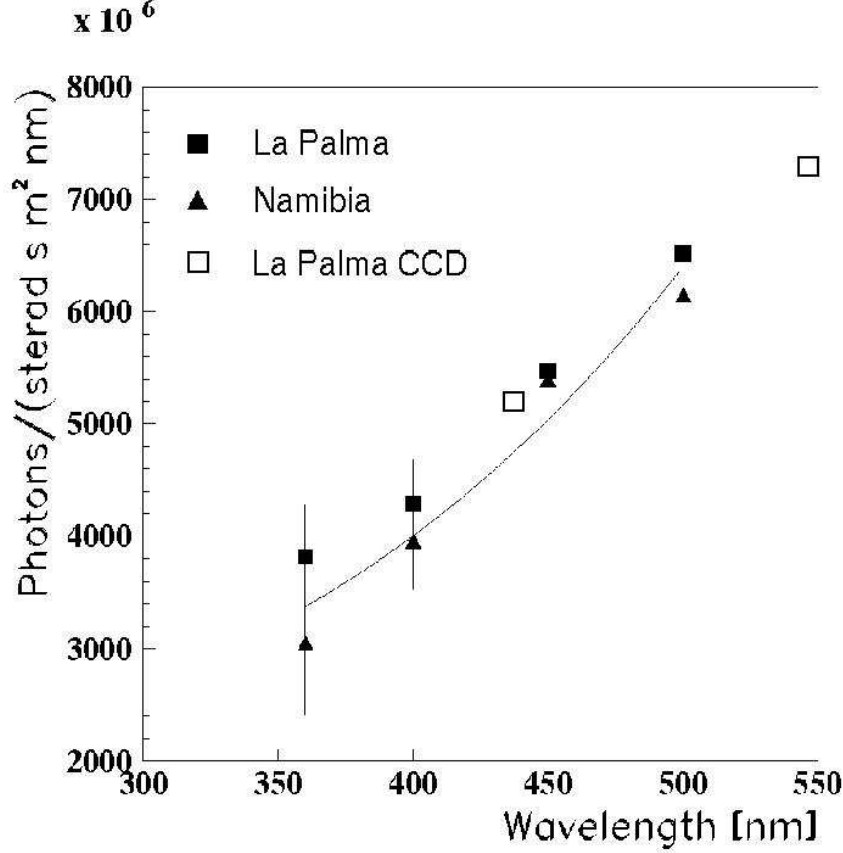
13

Fig. 8. Average differential photon flux in La Palma (full squares) and Namibia (triangles) from a set of dark regions near the zenith, as a function of wavelength. Also shown are the values of [3] for La Palma (open squares), see text for details.

In order to explore the variation of night sky brightness across the Milky Way, the range $-70° < l < 70°$ and $-30° < b < 30°$ was scanned in several nights, with step sizes varying between 5° for the regions of large $b$ and $l$, to 2° for the region of the galactic center. Fig. 11 illustrates the flux variation across the central region of the Milky Way. Fig. 12 shows in more detail the dependence of the photon flux on $b$, for different ranges of $l$, and also indicates the scatter of data points in each region. The galactic center region shows a prominent enhancement of photon flux, up to a factor 4 above the values obtained for dark regions of the sky. The flux peaks at $b \approx -5°$; the center region at $b = 0, l = 0$ is shadowed by dark clouds. Most of the scan points were taken at larger altitudes – the median altitude is 60° – and the observed variation of the photon flux should largely reflect a genuine dependence on $b$ and $l$, as opposed to artefacts resulting from the variation with $alt$ and $az$ of the zodiacal light and the light pollution from Windhoek. In particular, data for the center region, $|l| < 20°$ and small $|b|$, were taken avoiding the regions towards Windhoek and towards the zodiacal light. Selecting particularly 'clean' data sets, using only data at $alt > 60°$ or taken in the hours around midnight, the pattern remains unchanged.
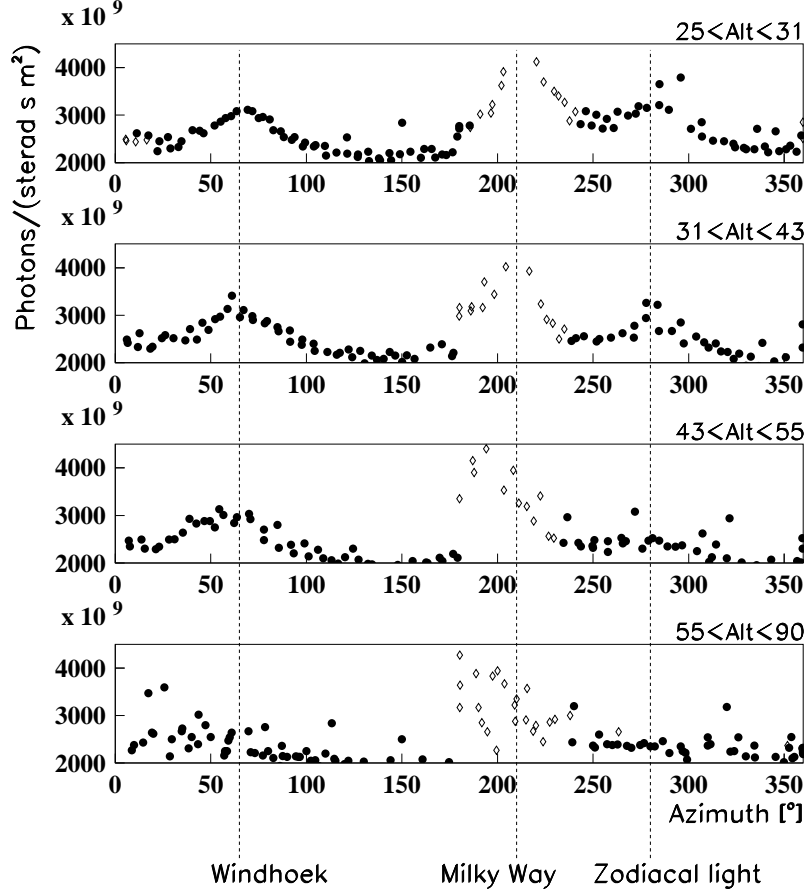
14

Fig. 9. Photon flux as a function of altitude and azimuth, for Namibia. Measurements were taken in 5° steps in azimuth starting at 25° altitude; after one complete turn, the altitude was incremented for the next azimuth scan. Open symbols denote the region of the Milky Way, with $|b| < 20°$. Scan points which contain stars brighter than 6 mag are not shown.

Averaging over scan points for altitude $> 60°$ and outside the galactic plane, $|b| > 20°$, and removing measurements with stars brighter than 6 mag. in the field of view, one finds a mean flux of

$$\phi = (2.21 \pm 0.22) \cdot 10^{12} \ \ \text{photons/sr s m}^2$$

for Namibia, and

$$\phi = (2.60 \pm 0.35) \cdot 10^{12} \ \ \text{photons/sr s m}^2$$

for La Palma, in the wavelength region from 300 nm to 650 nm. The errors quoted give the variation between different scan points, based on a Gaussian fit of the distribution. Statistical errors for the individual scan points are small. As mentioned earlier (Section 3), there is a 8.8% systematic error.
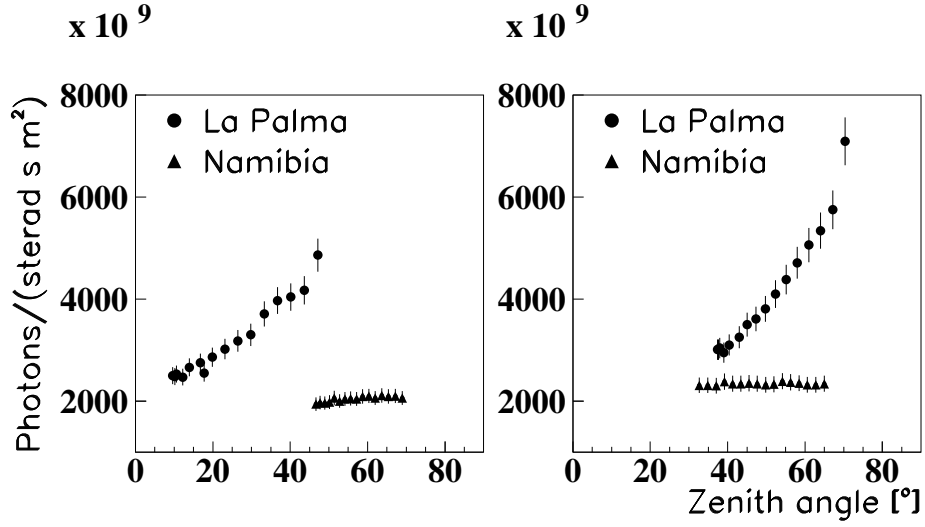
15

Fig. 10. Photon flux from two fixed locations of the sky (l=11.6°, b-71.4°, left and l=317°, b=53.4°, right) as a function of the zenith angle, for Namibia and La Palma.
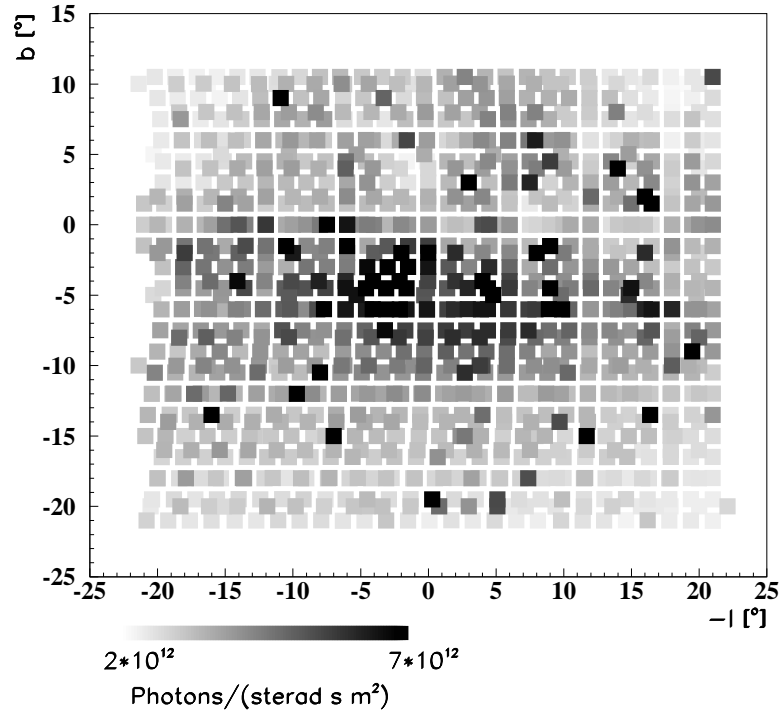


Fig. 11. Photon flux from the central region of the Galaxy, as a function of galactic longitude $l$ and latitude $b$. The squares represent individual scan points; the grey scale represents photon flux. Several scans with different step sizes are combined in the picture. Isolated points with very high flux indicate bright stars.

## 5 Measurement of the atmospheric transmission

In addition to the night-sky brightness, the atmospheric transmission was measured by following a star up to large zenith angles. Assuming constant
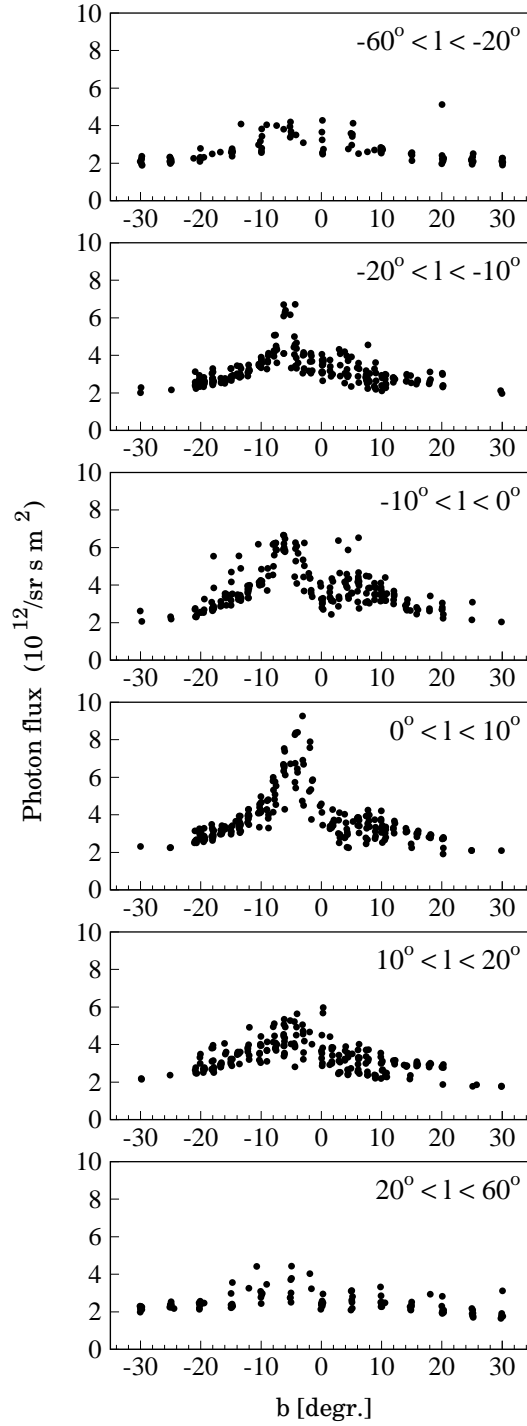
Fig. 12. Photon flux for different ranges in galactic longitude $l$, as a function of latitude $b$. Each point represents a scan point; scans were taken in several nights with a step size of typically $5°$ at large $b$ and $l$, and $2°$ for the center region. Point including stars brighter then 6 mag. are not shown. Statistical errors of the scan points are small; there is a common 8.8% systematic scale error.

absorption per unit airmass, the intensity to first order varies with the zenith angle $\theta_z$ as

$$\ln I(\theta_z) = -\tau \sec \theta_z + \ln I_0$$

where $\tau$ is the optical depth of the (vertical) atmosphere. Within errors, the transmission was identical on La Palma and in Namibia, with typical values of 60% at 360 nm, 72% at 400 nm, 80% at 450 nm and 84% at 500 nm, with errors of 3% to 4%.

## 6 Photoelectron rate in the PMTs of the H.E.S.S. telescopes, including albedo

The results discussed above show that the observation conditions at the Namibia site are indeed very good, with the night-sky flux slightly below the La Palma values for small zenith angles, and a nearly altitude-independent flux. Observations within the galactic plane and in particular near the galactic center will have to deal with an increase by a factor 4 in background levels. For the mirror area of about 94 m$^2$ of the H.E.S.S. telescopes (after accounting for the shadowing of the mirrors due to camera body and camera masts), and given the typical 80% mirror reflectivity, the 75% to 80% net transmission of the Winston cones in front of the PMTs, and the 0.16° pixel size of the H.E.S.S. cameras, one derives a background photoelectron rate per pixel of $85 \pm 13$ MHz for the average (non-galactic-plane) flux. Additional contributions to the background rate come from light rescattered from the ground, and from the structure of the telescope, which is visible between the round mirror tiles.

Using the identical setup, and pointing the instrument to the ground, the flux of rescattered night-sky background light was measured, and is summarized in Table 2. Weighting the rescattered night-sky background light from the ground with a reduced transmission of the Winston cones at larger angles, one finds that ground albedo will contribute a background photoelectron rate of $13 \pm 4$ MHz.

Concerning the telescope structure, the flux of backscattered light depends on the color of the telescope structure. Black color is obviously prefered, as far as night-sky background is concerned. On the other hand, white color reduces heating of the telescope structure during day time; in the sunshine, temperature differences of 15°C were measured between metal painted black and white. For the Cherenkov application, the important quantity is the reflectivity at short wavelengths, below 500 nm to 600 nm, where the sensitivity of the PMTs is high. The peak intensity of solar radiation heating the telescope structure during day time, on the other hand, is at longer wavelengths. A good compromise is therefore a red color, which absorbs most blue light and

| Material | Diffuse reflected night sky light (Photoel./sr s m$^2$) |
|---|---|
| Red sand | $(2.2 \pm 0.2) \cdot 10^{10}$ |
| Grass | $(2.5 \pm 0.2) \cdot 10^{10}$ |
| Black (RAL 9011) | $(1.3 \pm 0.1) \cdot 10^{10}$ |
| White (RAL 9010) | $(13.8 \pm 0.3) \cdot 10^{10}$ |
| Rose (RAL 3017) | $(3.4 \pm 0.1) \cdot 10^{10}$ |

Table 2
Diffuse reflected night sky light for different materials.

which reflects red light. Table 2 shows that indeed a red color (RAL 3017) is closer to black than to white as far as the background photoelectron yield is concerned; on the other hand, the temperature increase was measured to only 3°C, or 20% of the difference between black and white. The actual H.E.S.S. telescopes will be painted in a slightly darker red, RAL 3016, which should reduce the photoelectron yield by another factor 2. Weighted with the relevant solid angle, light scattered from the telescope structure is expected to contribute $2.4 \pm 1.2$ MHz of photoelectron rate, resulting in a total estimated background rate of $100 \pm 13$ MHz per pixel of the H.E.S.S. cameras.

## 7  Summary and conclusions

Using an instrument developed specially for this purpose, the level of the night sky background light was surveyed both at the La Palma site of the HEGRA Cherenkov telescope system, and near the site of the H.E.S.S. telescope system in Namibia. Measurements were carried out over typically 10 days at each location, under good weather conditions. For identical locations of the sky, measurements show a variation of 10% between nights. The average flux of dark regions of the night sky near the zenith in La Palma is $2.6 \cdot 10^{12}$ photons/sr s m$^2$, compared to $2.2 \cdot 10^{12}$ photons/sr s m$^2$ in Namibia, for a range between 300 and 650 nm. A remarkable feature of the Namibia data is that the flux from dark regions of the sky is independent of the zenith angle, for zenith angles up to at least 70°. Since the measurements essentially represent a snapshot, as compared to an annual average, it is not a priori clear to which extent long-term or seasonal variations can account for these differences; on the basis of visual observations over longer periods, the observation periods were characterized as representing fairly typical conditions.

Integrated over the field of view of the instrument (0.87°), the night sky background varies significantly with galactic longitude and latitude. The region near the galactic center shows fluxes which are increased by a factor 4 compared to dark regions of the sky, with consequences for the trigger thresholds

of Cherenkov telescopes observing in this region.

The instrument was also employed to study the effect of ground albedo and reflections from the structure of a Cherenkov telescope; for Cherenkov cameras where Winston cones properly limit the field of view of the individual pixels, the albedo contributions to the background photoelectron rate of pixel are below 20%.

# References

[1] F.E. Roach, J.L. Gordon, *The Light of the Night Sky*, D. Reidel Publishing Company 1973

[2] Ch. Leinert et al., Astron. Astrophys. Suppl. Ser. **127** (1998) 1

[3] C.R. Benn and S.L. Ellison, astro-ph/9909153, and *La Palma night–sky brightness*, La Palma technical note 115 (1998)

[4] R.H. Garstang, Pub. Astr. Soc. Pac. **101** (1989) 306

[5] F.A. Aharonian et al., *HESS (High Energy Stereoscopic System) — Letter of Intent*, 1997;
http://www-hfm.mpi-hd.mpg.de/HESS/HESS.html

[6] W. Hofmann, Proc. of the Workshop on TeV Gamma Ray Astrophysics, Towards a Major Atmospheric Cherenkov Detector V, Kruger Park, 1997, O.C. de Jager (Ed.), p. 405

[7] W. Hofmann, Proc. of the GeV-TeV Gamma Ray Astrophysics Workshop, Towards a Major Atmospheric Cherenkov Detector VI, Snowbird, 1999, B.L. Dingus, M.H. Salamon, D.B. Kieda (Eds.), AIP Conf. Proc. 515, p. 500

[8] T. Neckel, priv. comm.

[9] M. Sarazin, *An ESO-MPIA Site Survey: Technical notes on Gamsberg Namibian site*, ESO Notes, 1994/95,
http://www.eso.org/gen-fac/pubs/astclim/espas/gamsberg/index.html

[10] A. Daum et al., Astropart. Phys. **8** (1997) 1

[11] A. Konopelko et al., Astropart. Phys. **10** (1999) 275

[12] A. Kohnle et al., Nucl. Instr. Meth. **A 442** (2000) 322

[13] D.J. Buckley et al., Exp. Astr. **9** (1999) 237

[14] R. Mirzoyan und E. Lorenz, *Measurement of the Night Sky Light Background at La Palma*, MPI-PhE/94-35 (1994)

[15] S.R. Kaul et al., Bull. Astr. Soc. India **22** (1994) 133